Photodissociation of HI and DI: Testing models for electronic structure via polarization of atomic photofragments

David N. Jodoin and Alex Brown[a)]
Department of Chemistry, University of Alberta, Edmonton AB T6G 2G2, Canada

(Received 23 May 2005; accepted 7 June 2005; published online 5 August 2005)

The photodissociation dynamics of HI and DI are examined using time-dependent wave-packet techniques. The orientation and alignment parameters $\mathbf{a}_Q^{(K)}(p)$ are determined as a function of photolysis energy for the resulting ground-state $I(^2P_{3/2})$ and excited-state $I(^2P_{1/2})$ atoms. The $\mathbf{a}_Q^{(K)}(p)$ parameters describe the coherent and incoherent contributions to the angular momentum distributions from the $A\ ^1\Pi_1$, $a\ ^3\Pi_1$, and $t\ ^3\Sigma_1$ electronic states accessed by perpendicular excitation and the $a\ ^3\Pi_{0^+}$ state accessed by a parallel transition. The outcomes of the dynamics based on both shifted *ab initio* results and three empirical models for the potential-energy curves and transition dipole moments are compared and contrasted. It is demonstrated that experimental measurement of the $\mathbf{a}_Q^{(K)}(p)$ parameters for the excitation from the vibrational ground state ($\upsilon=0$) would be able to distinguish between the available models for the HI potential-energy curves and transition dipole moments. The differences between the $\mathbf{a}_Q^{(K)}(p)$ parameters for the excitation from $\upsilon=0$ stand in sharp contrast to the scalar properties, i.e., total cross section and I^* branching fraction, which require experimental measurement of photodissociation from excited vibrational states ($\upsilon>0$) to distinguish between the models. © *2005 American Institute of Physics*. [DOI: 10.1063/1.1989327]

I. INTRODUCTION

The hydrogen halides, H*X* (*X*=F, Cl, Br, and I), represent some of the simplest systems that dissociate to yield open-shell fragments. They provide model systems for studying molecular photodissociation dynamics on multiple potential-energy curves (PECs) including the effects of nonadiabatic coupling. In particular, the photodissociation process

$$HX + h\nu \rightarrow H(^2S) + X(^2P_{3/2})$$
$$\rightarrow H(^2S) + X(^2P_{1/2})$$

to yield the ground and spin-orbit excited-state halogen atoms has been of both experimental and theoretical interest.[1–35] Following standard nomenclature, the two spin-orbit states of the halogen atom, $X(^2P_{3/2})$ and $X(^2P_{1/2})$, are referred to as *X* and X^*, respectively. For HF, HCl, HBr, and HI, the spin-orbit splittings between the two product channels are 404, 882, 3685, and 7603 cm^{-1},[36] respectively, and thus, the effects of increasing spin-orbit coupling on the dissociation process can be examined systematically.

The goals of the experimental and theoretical studies have been to understand the roles of various electronic states involved in the excitation and the possible nonadiabatic transitions that could take place between the excited PECs as the molecule fragments. In order to achieve these goals, the more recent experimental and theoretical studies have focused on determining the branching fraction Γ, which provides the yield of spin-orbit excited atoms (X^*) relative to the total yield, and on the lowest-order ($K=0$) anisotropy parameter β, which provides information on the parallel and/or perpendicular nature of the electronic transitions contributing to the dissociation. While the measurement of the scalar properties, i.e., total cross section and Γ, and the lowest-order vector property β provide a wealth of information on the potential-energy curves, transition dipole moments, and, if applicable, nonadiabatic couplings underlying the dynamics, recent experiments[37–39] have determined the alignment of chlorine and bromine atoms resulting from the dissociation of HCl and HBr, respectively. Also, calculations of the alignment and orientation of the resulting halogen atoms have been carried out for the photodissociation of HF,[40] HCl,[38,41] and HI.[42] The resulting alignment and orientation are extremely sensitive to the details of the potential-energy curves and transition dipole moments and, as discussed in Sec. III for HI, provide more detailed information than measurement of the total cross section, branching fraction, or the anisotropy parameter β.

The halogen atoms can have a preferred orientation and/or alignment in space since they possess angular momenta. The spatial distribution of the photofragment angular momenta can be described by the contributions from dissociation on a single PEC and from the interference from dissociation via multiple PECs.[43] The $\mathbf{a}_Q^{(K)}(p)$ parameters[44] can fully describe the polarization of the resulting atomic photofragments in the molecular frame. *K* and *Q* refer to the spatial distributions in the molecular frame. The symmetry of the transition dipole moments from the ground electronic state to the dissociating states is given by *p* and can be $\parallel$, $\perp$, or ($\parallel$, $\perp$) corresponding to the pure parallel, pure perpendicular, or mixed parallel/perpendicular excitation. An equivalent set of anisotropy parameters describing the dissociation in the laboratory frame has also been introduced.[45,46]

[a)]Electronic mail: alex.brown@ualberta.ca

In the present work, the $\mathbf{a}_Q^{(K)}(p)$ parameters ($K \leqslant 3$) describing the alignment/orientation of iodine fragments, both I and I^*, produced from the photodissociation of HI and DI are reported. They are determined from a quantum-mechanical time-dependent wave-packet calculation based on recently published[21,22] empirical potential-energy curves and transition dipole moments as well as the best available *ab initio* data.[24] For the empirical models, the molecular parameters were determined by fitting the experimentally measured scalar properties, i.e., total cross section and branching fractions, for the HI and DI photofragmentation processes. Calculations based on them were then shown to reproduce the lowest-order anisotropy parameter β. The *ab initio* PECs and transition dipole moments have been shown[24,47,48] to reproduce the experimentally measured scalar properties. Here we demonstrate that measurement of the $\mathbf{a}_Q^{(K)}(p)$ parameters for the excitation from $\upsilon=0$ can distinguish between the various models for the electronic structure of HI.

The paper is organized in the following manner. Section II A outlines the underlying electronic structure as it relates to the two lowest-energy asymptotes $H(^2S_{1/2})+I(^2P_{3/2})$ and $H(^2S_{1/2})+I(^2P_{1/2})$, which are the only ones of interest here. A brief description of the $\mathbf{a}_Q^{(K)}(p)$ parameters relevant to HI (DI) dissociation is presented in Sec. II B. The methods used to determine the $\mathbf{a}_Q^{(K)}(p)$ parameters from a time-dependent wave-packet treatment of the dissociation dynamics are outlined in Sec. II B. The $\mathbf{a}_Q^{(K)}(p)$ parameters describing the $I(^2P_{3/2})$ and $I(^2P_{1/2})$ fragments arising from the photodissociation of HI from its vibrational ground state ($\upsilon=0$) are discussed in Sec. III A. In Sec. III B, the corresponding results for DI are presented and contrasted to those for HI. Finally, some conclusions and proposals for the experimental verification of these results are given in Sec. IV. The $\mathbf{a}_Q^{(K)}(p)$ parameters for vibrationally mediated photodissociation are also discussed, although detailed results are not presented here.

II. THEORY

The first step required in a theoretical investigation of photodissociation is to determine the underlying potential-energy curves or surfaces for polyatomic molecules, and the corresponding electronic transition dipole moments connecting the ground state to the excited electronic states. The couplings between the electronic states may also be required but the current models for HI do not invoke coupling between states. Once the electronic structure is known, a methodology for treating the dynamics is required and, in the present work, a time-dependent wave-packet treatment is utilized. From the dynamics, the photofragmentation **T**-matrix elements can be determined and used to obtain the $\mathbf{a}_Q^{(K)}(p)$ parameters via a well-established theoretical framework.[43,44,46,49] Since much of the theory has been presented elsewhere, including a detailed discussion for the photodissociation of HI,[42] each of these elements is discussed only briefly.

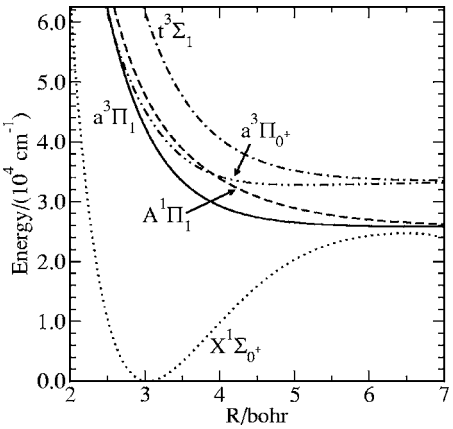

FIG. 1. The adiabatic potential-energy curves as a function of the HI bond length as determined using the data from Ref. 22 and corresponding to model 0. All potential energies are for $J=0$. The potentials, in order of increasing energy in the asymptotic region, are $X\,^1\Sigma_{0^+}$ (dotted line), $a\,^3\Pi_1$ (solid line), $A\,^1\Pi_1$ (dashed line), $a\,^3\Pi_{0^+}$ (dot-dot-dash line), and $t\,^3\Sigma_1$ (dot-dash line).

A. Electronic structure

The photodissociation of HI in the *A* band involves the excitation from the $X\,^1\Sigma_{0^+}$ ground state to four excited states: $A\,^1\Pi_1$, $a\,^3\Pi_1$, $a\,^3\Pi_{0^+}$, and $t\,^3\Sigma_1$. Figure 1 illustrates theadiabatic potential-energy curves, as determined in Ref. 22. The term symbols translate as a mixed Hund's case (a)/case (c) according to $^{2S+1}L_\Omega$. The ^{2S+1}L labels designate the largest case (a) contribution within the Franck-Condon region, see Table 3 of Ref. 24. For a molecule containing the heavy iodine atom, Hund's case (c) is more appropriate and Ω is the only good quantum number. The $A\,^1\Pi_1$ and $a\,^3\Pi_1$ states are accessed via perpendicular excitations ($\Delta\Omega=\pm1$), and these excited electronic states correlate with the H+I photofragmentation channel. On the other hand, the $a\,^3\Pi_{0^+}$ and $t\,^3\Sigma_1$ states that correlate with the $H+I^*$ channel are accessed via parallel ($\Delta\Omega=0$) and perpendicular ($\Delta\Omega=\pm1$) excitations, respectively. In general, the PECs and transition dipole moments for HI have been determined by fitting to experimental data[22,27,30,35,50–52] rather than from *ab initio* investigations—although *ab initio* calculations of the electronic structure of HI have been carried out.[24,53–55] Coupling between the electronic states has not been invoked in any of the fits except in the work of Levy and Shapiro.[30] Subsequently, the β parameter measurements[33] that Levy and Shapiro fit were shown to be incorrect.

In this paper, the recent empirical models[21,22] and *ab initio* predictions[24] for the PECs and associated transition dipole moments of HI are utilized. Three empirical models are considered: (1) the model arising from LeRoy's original analysis,[22] hereafter referred to as model 0, and (2) the two new models developed[21] to account for all original data and the recently measured branching ratios and anisotropy parameters β for the photolysis of HI($v=2,J=0$), hereafter referred to as models 1 and 2. The *ab initio* data for both PECs and transition dipole moments as determined by Alekseyev *et al.*[24] are also utilized and are referred to as the *ab initio* model. As suggested in Ref. 24, the $a\,^3\Pi_1$ and $a\,^3\Pi_{0^+}$ states are shifted upward by 500 cm^{-1}. In Ref. 47, the

TABLE I. Parameters defining the potential energy (in cm^{-1}) and transition dipole moment (in Debye) functions for model 0 (Ref. 22).

	$a^3\Pi_1$	$A^1\Pi_1$	$a^3\Pi_{0+}$	$t^3\Sigma_1^+$
Form	Exponential	Exponential	EMO	Exponential
r_x/Å	1.609	1.609	2.7	1.609
A_s/cm^{-1}	15714	21161	[a]	26890
$\beta_0/Å^{-1}$	2.949	2.128	1.54659	2.60
$\beta_1/Å^{-1}$	⋯	−0.30	0.067	⋯
$\beta_2/Å^{-1}$	⋯	⋯	−0.074	⋯
c_0 [b]	1.468	0.9368	1.014	0.93

[a]EMO potential form, Eq. (2), with a fixed well depth of D_e=600 cm^{-1}.
[b]Transition dipole moment defined as a cubic spline through the *ab initio* values from Ref. 24, multiplied by the scaling factor c_0.

$a\ ^3\Pi_1 \leftarrow X\ ^1\Sigma_{0^+}$ and $A\ ^1\Pi_1 \leftarrow X\ ^1\Sigma_{0^+}$ transition dipole moments are scaled by 1.05 to reduce the rms discrepancy between the calculations and experimental measurements for the I^* branching fraction for the excitation from υ=2. Since this effect is notably weaker than shifting the PECs, we have chosen to use the unscaled transition dipole moments for the *ab initio* model. The existing experimental data cannot distinguish between models 1 and 2 while model 0 does not properly account for the measurements from υ=2. The shifted *ab initio* data properly accounts for both the υ=0 measurements[24,48] and the υ=2 experiments.[47] Model 0 is included in order to compare the new results for the $\mathbf{a}_Q^{(K)}(p)$ parameters determined using model 1, model 2, and the *ab initio* model with those of the previous investigation.[42]

All three empirical models utilize the ground electronic potential-energy functions for HI and DI from Coxon and Hajigeorgiou.[56] The potential-energy functions for the excited $A\ ^1\Pi_1$, $a\ ^3\Pi_1$, and $t\ ^3\Sigma_1$ states are represented by the simple exponential function

$$V_{\exp}(r) = D_s + A_s \exp[-\beta(y_8)(r - r_x)]. \quad (1)$$

The $a\ ^3\Pi_{0^+}$ state is represented by the extended Morse oscillator (EMO) function

$$V_{\mathrm{EMO}} = [D_s - D_e] + D_e\{\exp[-\beta(y_8)(r - r_x)] - 1\}^2. \quad (2)$$

In Eqs. (1) and (2), D_s is the asymptotic energy of electronic state s. For the $A\ ^1\Pi_1$ and $a\ ^3\Pi_1$ states correlating with the ground-state iodine fragments, D_s is set at 25 778 cm^{-1}. For the $a\ ^3\Pi_{0^+}$ and $t\ ^3\Sigma_1$ states correlating with the excited-state iodine, D_s is 33 781 cm^{-1}. The difference between these asymptotic energies, 7603 cm^{-1}, reflects the spin-orbit splitting in atomic iodine. In Eq. (2), r_x is a reference distance, and the exponent coefficient $\beta(y_8)$ is defined as an expansion in the dimensionless radial variable $y_8=[r^8-r_x^8]/[r^8+r_x^8]$, i.e.,

$$\beta(y_8) = \beta_0 + \beta_1 y_8 + \beta_2 y_8^2 + \cdots. \quad (3)$$

In the EMO function used for the $a\ ^3\Pi_{0^+}$ state, the well depth of the shallow minimum, D_e, is fixed at 600 cm^{-1}.

The three empirical models use two types of transition dipole moment functions $\mu(r)$: (1) linearly scaled versions of the *ab initio* functions[24] and (2) empirical expansions in powers of the radial variable y_8:

TABLE II. Parameters defining the potential energy (in cm^{-1}) and transition dipole moment (in Debye) functions for model 1 (Ref. 21).

	$a^3\Pi_1$	$A^1\Pi_1$	$a^3\Pi_{0+}$	$t^3\Sigma_1^+$
Form	Exponential	Exponential	EMO	Exponential
r_x/Å	1.609	1.609	2.63892	1.609
A_s/cm^{-1}	15188	20873	[a]	27690
$\beta_0/Å^{-1}$	2.965	2.304	1.6323	2.60
$\beta_1/Å^{-1}$	⋯	−0.437	0.056	⋯
c_0	1.329[b]	0.978[b]	0.4072[c]	1.0[b]
c_1			0.069	

[a]EMO potential form, Eq. (2), with a fixed well depth of D_e=600 cm^{-1}.
[b]Transition dipole moment defined as a cubic spline through the *ab initio* values from Ref. 24, multiplied by the scaling factor c_0.
[c]Transition dipole moment defined by Eq. (4) with the coefficients c_0 and c_1.

$$\mu(r) = \sum_{i=0} c_i y_8^i. \quad (4)$$

The parameters defining the excited-state potential-energy curves and the transition dipole moment functions are given in Tables I, II, and III for models 0, 1, and 2, respectively.

In a recently published comment,[47] Alekseyev *et al.*, who generated the *ab initio* data we have used in this paper, speak strongly against model 2 being viable based on plausible physical reasoning. Firstly, in model 2, the $a\ ^3\Pi_{0^+}$ and $a\ ^3\Pi_1$ states lie notably lower than the corresponding *ab initio* potentials. This contradicts the argument based on the intrinsic properties of the computational method that these PECs should be shifted upwards in energy. Secondly, model 2 uses a $a\ ^3\Pi_{0^+} \leftarrow X\ ^1\Sigma_{0^+}$ transition dipole moment that increases with decreasing bond length. All computational methods indicate otherwise, i.e., the transition dipole moment decreases with decreasing bond length, see Fig. 3 of Ref. 24. For these reasons model 2 should most likely be discounted. So, while the primary comparison for the purposes of encouraging experiments to measure these parameters should be between model 1 and the *ab initio* model, calculations based on models 0 and 2 are included for completeness, and to demonstrate the sensitivity of the anisotropy parameters to differences in the PECs and transition dipole moments.

A detailed description of the correspondence between the photofragment atomic states and the adiabatic molecular

TABLE III. Parameters defining the potential energy (in cm^{-1}) and transition dipole moment (in Debye) functions for model 2 (Ref. 21).

	$a^3\Pi_1$	$A^1\Pi_1$	$a^3\Pi_{0+}$	$t^3\Sigma_1^+$
Form	Exponential	Exponential	EMO	Exponential
r_x	1.609	1.609	2.7	1.609
A_s/cm^{-1}	12823	20384	[a]	26830
$\beta_0/Å^{-1}$	2.495	2.945	1.51592	2.60
$\beta_1/Å^{-1}$	⋯	−0.260	⋯	⋯
c_0	0.8234[b]	0.46234[c]	0.4131[c]	1.00[b]
c_1		−0.613	−0.130	

[a]EMO potential form, Eq. (2), with a fixed well depth of D_e=600 cm^{-1}.
[b]Transition dipole moment defined as a cubic spline through the *ab initio* values from Ref. 24, multiplied by the scaling factor c_0.
[c]Transition dipole moment defined by Eq. (4) with the coefficients c_0 and c_1.

states is given in Ref. 40. The adiabatic treatment implies that four electronic states, i.e., the doubly degenerate $a\,^3\Pi_1$ and $A\,^1\Pi_1$ states, contribute to the angular distribution (orientation/alignment) of the ground-state $I(^2P_{3/2})$ fragment. These states correlate adiabatically as

$$\mathrm{HI}(a^3\Pi_1;\Omega' = \pm 1) \rightarrow \mathrm{H}(m_\mathrm{H} = \pm 1/2) + \mathrm{I}(m_\mathrm{I} = \pm 1/2) \tag{5}$$

and

$$\mathrm{HI}(A^1\Pi_1;\Omega' = \pm 1) \rightarrow \mathrm{H}(m_\mathrm{H} = \mp 1/2) + \mathrm{I}(m_\mathrm{I} = \pm 3/2). \tag{6}$$

Within the present adiabatic models for the photodissociation, the ground-state $X\,^1\Sigma_{0^+}$ does not contribute to the production of $I(^2P_{3/2})$. However, in principle, this state could gain population via nonadiabatic recoupling from the $a\,^3\Pi_{0^+}$ state—although experimental measurements[26,27,29,31,34,35] of β suggest that there is no parallel contribution to the production of $I(^2P_{3/2})$.

Three excited states, i.e., the nondegenerate $a\,^3\Pi_{0^+}$ state and the doubly degenerate $t\,^3\Sigma_1$ state, contribute to the angular distribution of the excited state $I(^2P_{1/2})$ fragment. The $a\,^3\Pi_{0^+}$ state correlates equally with both $m_\mathrm{H} = \pm 1/2$ and $m_{\mathrm{I}^*} = \mp 1/2$ states, i.e.,

$$\mathrm{HI}(a^3\Pi_{0^+};\Omega' = 0) \rightarrow \mathrm{H}(m_\mathrm{H} = \pm 1/2) + \mathrm{I}^*(m_\mathrm{I} = \mp 1/2). \tag{7}$$

The $t\,^3\Sigma_1$ state correlates as

$$\mathrm{HI}(t^3\Sigma_1;\Omega' = \pm 1) \rightarrow \mathrm{H}(m_\mathrm{H} = \pm 1/2) + \mathrm{I}^*(m_\mathrm{I} = \pm 1/2). \tag{8}$$

The molecular wave functions corresponding to these asymptotes are given in Table II of Ref. 40. The long-range correlations given in Eqs. (5)–(8) are required for the determination of the orientation and alignment parameters, $\mathbf{a}_Q^{(K)}(p)$.

B. Determination $\mathbf{a}_Q^{(K)}(p)$ parameters via time-dependent wave-packet dynamics

The primary goal of this work is to determine the $\mathbf{a}_Q^{(K)}(p)$ parameters describing the orientation and alignment of the iodine atomic fragments in the molecular frame. The theoretical and/or experimental determination of $\mathbf{a}_Q^{(K)}(p)$ parameters provides the most detailed understanding of the photodissociation dynamics. For these parameters, K and Q refer to the spatial distribution in the molecular frame and p refers to the symmetry of the transition connecting the ground electronic state to the dissociative excited states. The symmetry p can be pure perpendicular ($\perp$), pure parallel ($\parallel$), or mixed parallel/perpendicular ($\parallel,\perp$). The scalar and lowest-order vector properties, including the total cross section, the I^* branching fraction, and the anisotropy parameter β, have been determined previously for these PECs and transition dipole moments.[21,22,24,47,48] Therefore, we do not discuss these parameters in the present work.

In the following description of the anisotropy parameters, the nuclear spins of the photofragments have been neglected. Since the duration of the dissociation process is typically much smaller than the Heisenberg uncertainty time $\Delta t = \hbar/(2\Delta E)$ associated with the hyperfine splitting in the atoms, this assumption is justified. While the nuclear spins do not affect the photodissociation dynamics, the hyperfine interaction in the final fragments results in the partial depolarization of the fragment's electron angular momenta.[57] For the dissociation of the HI molecule considered here, any orbital alignment of the I-atom photofragment will degrade to $\approx 23\%$ of its nascent value through coupling with the $I = 5/2$ nuclear spin.

The dimensionless anisotropy parameters $\mathbf{a}_Q^{(K)}(p)$ are normalized combinations of the dynamical functions $f_K(q,q')$. For the dissociation of HI resulting in the production of iodine and hydrogen atoms having angular momenta j_I and j_H, respectively, the dynamical functions for the iodine atom are defined as

$$\begin{aligned} f_K(q,q') = \sum_{n,\Omega,\Omega_\mathrm{I},n',\Omega',\Omega_\mathrm{I}'} & (-1)^{K+j_\mathrm{I}+\Omega_\mathrm{I}'} \begin{pmatrix} j_\mathrm{I} & j_\mathrm{I} & K \\ -\Omega_\mathrm{I} & \Omega_\mathrm{I}' & q-q' \end{pmatrix} \\ & \times (T^{n\Omega}_{j_\mathrm{I}\Omega_\mathrm{I} j_\mathrm{H}\Omega_\mathrm{H}})^* T^{n'\Omega'}_{j_\mathrm{I}\Omega_\mathrm{I}' j_\mathrm{H}\Omega_\mathrm{H}} \\ & \times \langle \Psi^-_{n,\Omega}(R,E)|\hat{\mathbf{d}}_q|\Psi_{\Omega_i}\rangle^* \langle \Psi^-_{n',\Omega'}(R,E)|\hat{\mathbf{d}}_{q'}|\Psi_{\Omega_i}\rangle. \end{aligned} \tag{9}$$

The expression $\langle \Psi^-_{n,\Omega}(R,E)|\hat{\mathbf{d}}_q|\Psi_{\Omega_i}\rangle$ is the energy-dependent photofragmentation $\mathbf{T}$-matrix element associated with channel n and is the critical quantity that must be determined from the dynamics calculation (see below). The indices q and q' are the vector spherical harmonic components[57,58] of the molecular electric dipole moment with respect to the recoil axis. These indices can take the value of 0 corresponding to a parallel electronic transition or the values ± 1 corresponding to perpendicular electronic transitions. The initial and final z components of the total electronic angular momentum about the molecular axis are related by $\Omega = \Omega_i + q$. The diagonal elements of the dynamical functions $f_K(q,q')$ with $q = q'$ correspond to incoherent excitation of perpendicular or parallel transitions. The off-diagonal elements with $q \neq q'$ correspond to coherent excitation of different molecular continua. The expression for the dynamical functions for the hydrogen atom can be obtained from Eq. (9) by exchanging the subscripts I and H.

For the ground-state iodine photofragments $I(^2P_{3/2})$, the relevant dynamical functions range from $K = 0$ to 3, while for the excited-state iodine $I(^2P_{1/2})$, they correspond to $K = 0$ or 1. Since the dynamical functions are directly related to the angular momentum state multipoles,[40] K is referred to as the multipole rank. For the ground-state iodine fragment, the complete set of state multipoles (dynamical functions) contains $K = 0$ (population), $K = 1$ (orientation, dipole moment), $K = 2$ (alignment, quadrupole moment) and $K = 3$ (orientation, octopole moment). The description for the excited-state iodine fragment requires only $K = 0$ and $K = 1$ dynamical functions.

In order to clarify the meaning of the anisotropy parameters that are utilized for describing the ground-state iodine $I(^2P_{3/2})$ and the excited-state iodine $I(^2P_{1/2})$ fragments, their relationships to the dynamical functions are described below. The zeroth-rank ($K=0$) anisotropy parameter is the well-known β parameter and is given by[43]

$$\beta = \frac{2[f_0(0,0) - f_0(1,1)]}{2f_0(1,1) + f_0(0,0)}. \tag{10}$$

The β parameters for the iodine atoms are not discussed here as they have been examined previously for models 0, 1, and 2 (Refs. 21 and 22) and for the *ab initio* model.[24] The ground-state I-atom products result exclusively from the perpendicular transitions to the $a^3\Pi_1$ and $A^1\Pi_1$ states and $\beta=-1$ independent of the photolysis energy. On the other hand, the I^* products result primarily from the parallel transition to the $a^3\Pi_{0^+}$ state below 50 000 cm^{-1} and from the perpendicular transition to $t^3\Sigma_1$ above 50 000 cm^{-1}. Thus, the β parameter describing the production of I^* changes from +2 at low energies to −1 at high energies.

As in our previous study of HI and DI based on model 0,[42] the $\mathbf{a}_0^{(1)}(\perp)$, $\mathbf{a}_0^{(2)}(\perp)$, $\mathbf{a}_0^{(3)}(\perp)$, $\mathbf{a}_2^{(2)}(\perp)$, and $\mathbf{a}_2^{(3)}(\perp)$ anisotropy parameters are computed for the ground-state fragments, and the $\mathbf{a}_0^{(1)}(\perp)$ and $\mathbf{a}_1^{(1)}(\parallel,\perp)$ parameters are determined for the excited-state fragments. The $\mathbf{a}_0^{(K)}(\perp)$ parameters describe the incoherent perpendicular excitation, the $\mathbf{a}_2^{(K)}(\perp)$ parameters describe the coherent perpendicular excitation, and the $\mathbf{a}_1^{(1)}(\parallel,\perp)$ parameter describes the coherent parallel and perpendicular excitation. In principle, there are additional parameters describing the coherent parallel and perpendicular excitations for the production of ground-state iodine, i.e., $\mathbf{a}_Q^{(K)}(\parallel,\perp)$, $2\leqslant K\leqslant 3$. However, within the present adiabatic treatment of the dynamics, there is no parallel contribution to $I(^2P_{3/2})$ fragments and therefore all $\mathbf{a}_Q^{(K)}(\parallel,\perp)$ parameters are identically zero. Only a single state accessed by parallel excitation correlates with the excited-state asymptote, and thus no parallel only parameters $\mathbf{a}_Q^{(K)}(\parallel)$ are computed. Since the role of the $t^3\Sigma_1$ state is negligible in *A* band, the previous *ab initio* studies[24] have omitted it from discussions and we choose to do the same for the *ab initio* model in the present work. Hence, only results for the parameters describing ground-state iodine fragments are presented based on the *ab initio* PECs and transition dipole moments.

The parameters describing the incoherent perpendicular excitation are related to the dynamical functions Eq. (9) by

$$\mathbf{a}_0^{(1)}(\perp) = \frac{f_1(1,1)}{f_0(1,1)}, \tag{11}$$

$$\mathbf{a}_0^{(2)}(\perp) = V_2(j_I)^{-1}\frac{f_2(1,1)}{f_0(1,1)}, \tag{12}$$

and

$$\mathbf{a}_0^{(3)}(\perp) = V_3(j_I)^{-1}\frac{f_3(1,1)}{f_0(1,1)}. \tag{13}$$

For the ground-state iodine photofragment, the parameters $V_2(j_I)$ and $V_3(j_I)$ are given by

$$V_2(j_I = 3/2) = \left[\frac{j_I(j_I+1)}{(2j_I+3)(2j_I-1)}\right]^{1/2} = \frac{\sqrt{15}}{4\sqrt{3}} \tag{14}$$

and

$$V_3(j_I = 3/2) = \frac{j_I(j_I+1)}{[(j_I-1)(j_I+2)(2j_I-1)(2j_I+3)]^{1/2}} = \frac{15}{4\sqrt{21}}. \tag{15}$$

Since $K=0$ or 1 for the excited-state iodine fragment $I(^2P_{1/2})$, only the $\mathbf{a}_0^{(1)}(\perp)$ parameter is required for the description of incoherent perpendicular excitation.

The description of the angular distribution of the ground-state $I(^2P_{3/2})$ fragment also requires two parameters for coherent perpendicular excitation, i.e.,

$$\mathbf{a}_2^{(2)}(\perp) = -\frac{1}{2}V_2(j_I)^{-1}\frac{f_2(1,-1)}{f_0(1,1)} \tag{16}$$

and

$$\mathbf{a}_2^{(3)}(\perp) = \frac{i}{2}V_3(j_I)^{-1}\frac{f_3(1,-1)}{f_0(1,1)}. \tag{17}$$

For the excited-state iodine fragment, the parameter $\mathbf{a}_1^{(1)}(\parallel,\perp)$ describing coherent parallel and perpendicular excitations is

$$\mathbf{a}_1^{(1)}(\parallel,\perp) = \frac{-3\sqrt{2}f_1(1,0)}{2f_0(1,1) + f_0(0,0)}. \tag{18}$$

The parameter describing coherent parallel and perpendicular excitations usually has its real and imaginary parts presented separately.[44]

In order to determine the dynamical functions required to calculate the anisotropy parameters, the photofragmentation **T**-matrix elements must be obtained from the dynamics. A time-dependent wave-packet formulation for the dynamics[59–64] is used in the present work. The time-dependent approach is based upon the solution of the nuclear Schrödinger equation

$$i\hbar\frac{\partial\Phi(R,t)}{\partial t} = \hat{H}(R)\Phi(R,t) = \left[-\frac{\hbar^2}{2\mu}\frac{d^2}{dR^2} + V(R)\right]\Phi(R,t). \tag{19}$$

In Eq. (19), μ is the reduced mass of the molecule, $\Phi(R,t)$ is a column vector describing the time-dependent wave function on each of the excited electronic states of the molecule, and $V(R)$ is a diagonal matrix of the adiabatic potential energies. No off-diagonal couplings are considered in the present adiabatic treatment of the dynamics. The rotational part of the nuclear kinetic-energy operator is neglected in Eq. (19). As in our previous studies of hydrogen halide dissociation,[2,4,40,65] the axial recoil approximation is assumed to be valid, which is equivalent to the neglect of the overall rotation of the molecule.[66]

In the time-dependent approach, initial wave-packet packets $\phi_n(R,t=0)$ are prepared by multiplying the initial nuclear vibrational wave function of the molecule, $\psi_{\Omega_i}(R)$,

by the corresponding adiabatic transition dipole moment between the ground state and the nth excited state $d^n_{q'}(R)$. The index q' is the vector spherical harmonic component of the transition dipole moment function and it is determined by the symmetries of the ground and excited electronic states. The initial ground-state nuclear wave functions have been determined using the Fourier grid Hamiltonian method.[59,67,68] Once the initial wave packets are defined, they are propagated in time under the influence of the excited-state potential-energy surfaces. The time propagation is performed using the Chebychev expansion technique.[69,70]

In order to determine the photofragmentation **T**-matrix elements, the time-evolving wave packets are analyzed at each time step as they pass through an analysis line defined at a large fixed value of the bond length ($R=R_\infty$). By taking the Fourier transform over time of these cuts through the time-dependent wave packets $\phi_n(R_\infty,t)$, energy-dependent coefficients[2,4,60] $A_n(R_\infty,E)$ are then obtained, where

$$A_n(R_\infty,E)=\frac{1}{2\pi}\int_0^\infty \phi_n(R_\infty,t)\exp[i(E_i+h\nu)t/\hbar]dt. \qquad (20)$$

As has been discussed previously,[40,60] the photofragmentation **T**-matrix elements are related to these energy-dependent coefficients by

$$\langle \Psi^-_{n,\Omega}(R,E)|\hat{\mathbf{d}}_q|\Psi_{\Omega_i}\rangle = i\left(\frac{h^2k_v}{2\pi\mu}\right)^{1/2}\exp(-ik_vR_\infty)A_n(R_\infty,E). \qquad (21)$$

Once the **T**-matrix elements are known, the dynamical functions $f_K(q,q')$ can be determined via Eq. (9), and then the anisotropy parameters can be obtained using the relationships given in Eqs. (11)–(18).

III. RESULTS AND DISCUSSION

In the following sections, the focus is on the determination of the anisotropy parameters $\mathbf{a}^{(K)}_Q(p)$ within the current adiabatic models[21,22,24] for dissociation. The calculations demonstrate that the experimental measurement of these parameters for the excitation from $v=0$ can distinguish between the current empirical models and the *ab initio* results. In order to distinguish between the present models via scalar properties, e.g., the total cross section or the I^* branching fraction, measurements must be made for $v>0$ using vibrationally mediated photodissociation.[21] The measurement of the $\mathbf{a}^{(K)}_Q(\perp)$ parameters allows the determination of the relative roles of the $a^3\Pi_1$ and $A^1\Pi_1$ states. The relative contributions of these states cannot be determined via measurement of either the I^* branching fraction, since both correlate with ground-state fragments or the β parameter, since both are accessed via perpendicular transitions. The sensitivity of the $\mathbf{a}^{(1)}_1(\parallel,\perp)$ parameter to the relative amounts of parallel and perpendicular excitation is also demonstrated.

A. Anisotropy parameters for iodine fragments from the dissociation of HI

The angular distribution for the ground-state iodine fragment $I(^2P_{3/2})$ is described by both orientation ($K=1$ and $K=3$) and alignment ($K=2$) parameters. On the other hand, the excited-state $I(^2P_{1/2})$ fragment's angular distribution is fully described by orientation ($K=1$) parameters only. The anisotropy parameters determined from the four models for the electronic structure are discussed first for the ground-state iodine fragment and then for the excited-state atom. The primary comparison is between the results based on model 1 and the *ab initio* model, as model 0 has been discounted due to its inability to reproduce the results of the vibrationally mediated photodissociation experiments,[21] while model 2 is unlikely due to physical arguments based on the best available *ab initio* results.[47] However, the results based on these latter two models are included for comparison and to demonstrate the sensitivity of the $\mathbf{a}^{(K)}_Q(\perp)$ parameters to changes in the PECs and the transition dipole moments. It should be noted that when dissociating with linearly polarized light, the spatial distribution of the angular momentum of the ensemble of $I(^2P_{1/2})$ photofragments is dependent only on the $\mathbf{a}^{(2)}_0(\perp)$ and $\mathbf{a}^{(2)}_2(\perp)$ parameters as the excitation is of perpendicular character only. On the other hand, when dissociating with circularly polarized light, the angular distribution of the iodine fragments reflects contributions from the odd K parameters.[44] Thus, while all of the $\mathbf{a}^{(K)}_Q(\perp)$ parameters may be determined from our calculations, their measurement requires experiments with both linearly and circularly polarized light.

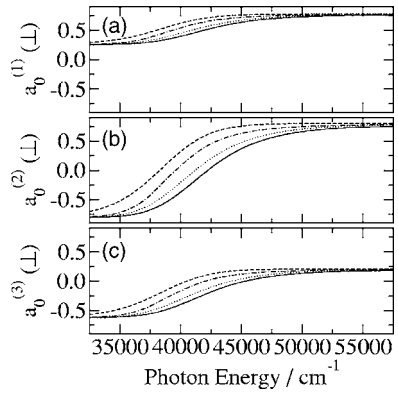

FIG. 2. Incoherent anisotropy parameters (a) $\mathbf{a}^{(1)}_0(\perp)$, (b) $\mathbf{a}^{(2)}_0(\perp)$, and (c) $\mathbf{a}^{(3)}_0(\perp)$, for the production of ground state $I(^2P_{3/2})$ as a function of photon energy for the photodissociation of HI initially in the rotationless ground ($v=0$) vibrational state. The results were determined from model 0 (solid line), model 1 (dotted line), model 2 (dashed line), and the *ab initio* model (dot-dash line), respectively.

Figure 2 illustrates the anisotropy parameters describing the incoherent perpendicular excitation, $\mathbf{a}^{(K)}_0(\perp)$, for the ground-state $I(^2P_{3/2})$ fragment produced from the photodissociation of HI as a function of photolysis wavelength. The results are for the excitation from the rotationless ground ($v=0$) vibrational state. Results are presented for the three empirical models and the *ab initio* model. As discussed in Sec. II A, the primary comparison is between model 1 and the *ab initio* model and Fig. 2 illustrates that there are clear differences between the $\mathbf{a}^{(K)}_0(\perp)$ parameters for these two models. For example, the difference between $\mathbf{a}^{(2)}_0(\perp)$ for model 1 and the *ab initio* model is greater than 0.1 for photolysis energies between 37 000 and 47 000 cm^{-1} and the maximum difference of 0.26 occurs at approximtely

41 000 cm^{-1}. For HCl and HBr, the $\mathbf{a}_0^{(K)}(\perp)$ parameters for $K=1$ and 2 have been measured[37,38] with an uncertainty of ±0.2 and, thus, which of the models, if either, provide a correct prediction should be amenable to experimental measurement. Also, the measurements[21,23,25–29,31,32,35] of the I^* branching fractions and β parameters have been made between 34 772 and 48 780 cm^{-1} indicating that the energy range exhibiting the largest difference between the models is accessible experimentally.

Within the adiabatic model of dissociation, the $\mathbf{a}_0^{(K)}(\perp)$ parameters are directly related to the excitation probability to, and relative yields from, the $A^1\Pi_1$ and $a^3\Pi_1$ states.[40] Therefore, the differences in the $\mathbf{a}_0^{(K)}(\perp)$ parameters reflect the differences in the energies of these two excited states and the magnitudes of the transition dipole moments to the two states. In fact, the low-energy and high-energy limiting values of the $\mathbf{a}_0^{(K)}(\perp)$ parameters reflect the near 100% yield with respect to the total I production from $a^3\Pi_1$ (0% yield from $A^1\Pi_1$) at low energies and the 0% (100%) yield at high energies. The fact that the transition between the limiting values of the $\mathbf{a}_0^{(K)}(\perp)$ parameters occurs at higher energy for model 1 versus the *ab initio* model can primarily be attributed to the scaling of the transition dipole moments; the PECs are very similar, see Fig. 10 of Ref. 22. For model 1, the *ab initio* transition dipole moment to the $a^3\Pi_1$ state is scaled by 1.329, increasing its contribution at all photolysis energies. On the other hand, the transition dipole moment to $A^1\Pi_1$ is scaled by 0.978, and therefore, the contribution of this state is very similar for both model 1 and the *ab initio* model. The similarities between the results for models 0 and 1 are not surprising given that the PECs and transition dipole moments for the $a^3\Pi_1$ and $A^1\Pi_1$ states are very similar, see Tables I and II. The significant difference between model 2 and the other models reflects two phenomena. First, there is a much larger difference between the vertical excitation energies to the $a^3\Pi_1$ and $A^1\Pi_1$ states as compared to other models, i.e., ≈7600 cm^{-1} for model 2 versus ≈5500 cm^{-1} for other models. Second, model 2 decreases the contribution of the $a^3\Pi_1$ state by scaling the *ab initio* transition dipole moment by 0.8234 and has a completely different functional form of the transition dipole moment to the $A^1\Pi_1$ state, which increases its contribution at lower photolysis energies.

The $\mathbf{a}_2^{(K)}(\perp)$ parameters describing the coherent perpendicular excitation of the $a^3\Pi_1$ and $A^1\Pi_1$ states are illustrated in Fig. 3 for the $I(^2P_{3/2})$ fragment arising from the photodissociation of HI from the rotationless ground ($v=0$) vibrational state. The $\mathbf{a}_2^{(2)}(\perp)$ parameter describes the degree of coherence between pairs of m states, m and $m\pm2$. The magnitude of the $\mathbf{a}_2^{(K)}(\perp)$ parameters is related to the relative probability of excitation into the $a^3\Pi_1$ or $A^1\Pi_1$ excited states within the adiabatic model for dissociation. On the other hand, the sign of the $\mathbf{a}_2^{(K)}(\perp)$ parameters depends on the phase difference between the photofragmentation **T**-matrix elements for the $a^3\Pi_1$ and $A^1\Pi_1$ states. The theoretically determined parameters depend strongly on the photolysis energy over the entire energy range except for the $\mathbf{a}_2^{(2)}(\perp)$ parameter determined from the *ab initio* model. More importantly, the dependence on the photolysis energy is different

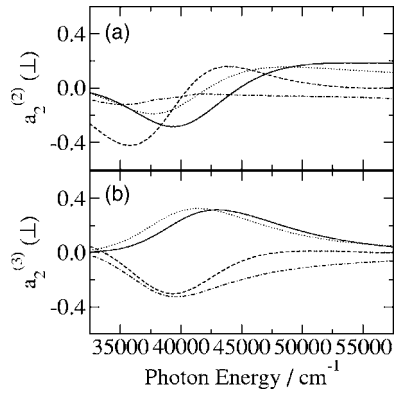

FIG. 3. Coherent anisotropy parameters (a) $\mathbf{a}_2^{(2)}(\perp)$ and (b) $\mathbf{a}_2^{(3)}(\perp)$ for the production of ground state $I(^2P_{3/2})$ as a function of photon energy for the photodissociation of HI initially in the rotationless ground ($v=0$) vibrational state. The results were determined from model 0 (solid line), model 1 (dotted line), model 2 (dashed line), and the *ab initio* model (dot-dash line), respectively.

for the three empirical and the *ab initio* models of the electronic structure.

Only a single state ($^3\Sigma_{\Omega=+1}$ or $^3\Sigma_{\Omega=-1}$) accessed by perpendicular excitation contributes to the photofragmentation cross section for excited state $I(^2P_{1/2})$ production. Therefore, the $\mathbf{a}_0^{(1)}(\perp)$ parameter is equal to the maximal value of 0.577 ($=1/\sqrt{3}$), independent of the photolysis energy, and is not plotted. The particular state involved depends upon whether right- or left-circularly polarized light is utilized in the dissociation;[38] recall that only dissociation with circularly polarized light is sensitive to the odd K parameters. Note that while the role and energetics of $t^3\Sigma_1$ have not been assessed for the *ab initio* model, the value of $\mathbf{a}_0^{(1)}(\perp)$ will still be 0.577 independent of the photolysis energy.

The $\mathrm{Re}[\mathbf{a}_1^{(1)}(\parallel,\perp)]$ and $\mathrm{Im}[\mathbf{a}_1^{(1)}(\parallel,\perp)]$ parameters describing the coherent parallel and perpendicular excitations are plotted in Fig. 4 for all three empirical models. As discussed in Sec. II A, the previous studies of HI photodissociation based on the *ab initio* PECs and transition dipole moments have omitted the $t\,^3\Sigma_1$ state from discussions as it only contributed in the high-energy region, i.e.,

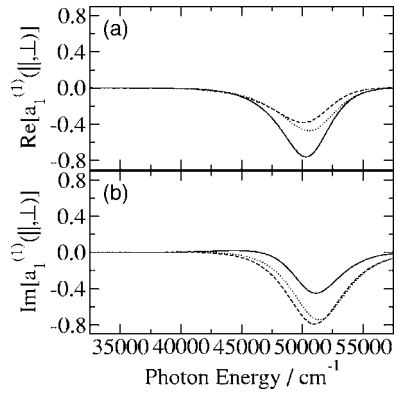

FIG. 4. Coherent anisotropy parameters (a) $\mathrm{Re}[\mathbf{a}_1^{(1)}(\parallel,\perp)]$ and (b) $\mathrm{Im}[\mathbf{a}_1^{(1)}(\parallel,\perp)]$ for the production of excited state $I(^2P_{1/2})$ as a function of photon energy for the photodissociation of HI initially in the rotationless ground ($v=0$) vibrational state. The results were determined from model 0 (solid line), model 1 (dotted line), and model 2 (dashed line), respectively.

$>50\,000\ \mathrm{cm}^{-1}$. According to the *ab initio* calculations,[24] the onset of the $t\ ^3\Sigma_1 \leftarrow X\ ^1\Sigma_{0^+}$ absorption is underestimated. In addition, the data suggest that a diabatic representation may be more appropriate for describing the $t\ ^3\Sigma_1$ transition. For these reasons, this state was omitted in the discussion of the photodissociation in the original paper[24] and we choose to omit it here for the *ab initio* model. Hence, no $\mathbf{a}_1^{(1)}(\parallel,\perp)$ parameters are determined for the *ab initio* model. For the empirical models, the $\mathbf{a}_1^{(1)}(\parallel,\perp)$ parameters show a strong dependence on the photolysis energy in the region where excitations to both $a\ ^3\Pi_{0^+}$ and $t\ ^3\Sigma_1$ are feasible, i.e., approximately $41\,000-56\,000\ \mathrm{cm}^{-1}$.

As discussed in Ref. 42, the $\mathbf{a}_1^{(1)}(\parallel,\perp)$ parameters are more sensitive to the amount of parallel and perpendicular excitations than the corresponding β parameters. Experimental measurements of the $\mathbf{a}_1^{(1)}(\parallel,\perp)$ parameters below approximately $45\,000\ \mathrm{cm}^{-1}$ should be able to provide evidence for or against the possibility of nonadiabatic coupling between the $t\ ^3\Sigma_1$ state and the $a\ ^3\Pi_1$ and $A\ ^1\Pi_1$ states. It is clear that direct excitation to $t\ ^3\Sigma_1$ is not feasible in that energy range,[24] see Fig. 1, and therefore, any perpendicular contribution to the I^* dissociation channel must be from nonadiabatic coupling. Measurement of the $\mathbf{a}_1^{(1)}(\parallel,\perp)$ parameters would also allow a more definitive assignment of the energy of the $t\ ^3\Sigma_1$ state and will help in the refinement of the electronic structure models.

From the results of Figs. 2–4 it is clear that the experimental measurement of the $\mathbf{a}_Q^{(K)}(p)$ parameters for the iodine fragment resulting from HI photodissociation would provide an alternative to the measurement of scalar properties from vibrationally mediated photodissociation as a mean to distinguish between the empirical models, and, of course, to determine the accuracy of the *ab initio* results. It may also be useful to measure the $\mathbf{a}_Q^{(K)}(p)$ parameters for the deuterated species DI as this would provide an additional test for the empirical models and the *ab initio* data. The results for DI are discussed below.

B. Anisotropy parameters for iodine fragments from the dissociation of DI

The $\mathbf{a}_0^{(K)}(\perp)$ anisotropy parameters as a function of photolysis wavelength for the ground-state $I(^2P_{3/2})$ fragment produced from the photodissociation of DI in its rotationless ground $(v=0)$ vibrational state are shown in Fig. 5. Figure 5 shows that there are significant similarities in the behavior of the $\mathbf{a}_0^{(K)}(\perp)$ parameters as a function of photolysis frequency for the $I(^2P_{3/2})$ produced from HI and DI. In fact, as was shown for model 0 previously,[42] these differences for a given model are less than or equal to the typical error bars associated with the experimental measurement of $\mathbf{a}_0^{(K)}(\perp)$ parameters. On the other hand, as with the $\mathbf{a}_0^{(K)}(\perp)$ parameters for HI dissociation, see Fig. 2, the differences between model 1 and the *ab initio* model should be experimentally detectable. For example, the maximum difference between the $\mathbf{a}_0^{(2)}(\perp)$ parameter for model 1 and the *ab initio* model is 0.30 and occurs at $41\,289\ \mathrm{cm}^{-1}$. The $\mathbf{a}_0^{(K)}(\perp)$ anisotropy parameters predicted for HI and DI for all electronic structure models are in marked contrast to those calculated for HCl and DCl

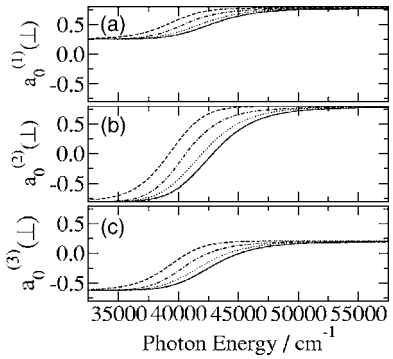

FIG. 5. Incoherent anisotropy parameters (a) $\mathbf{a}_0^{(1)}(\perp)$, (b) $\mathbf{a}_0^{(2)}(\perp)$, and (c) $\mathbf{a}_0^{(3)}(\perp)$, for the production of ground state $I(^2P_{3/2})$ as a function of photon energy for the photodissociation of DI initially in the rotationless ground $(v=0)$ vibrational state. The results were determined from model 0 (solid line), model 1 (dotted line), model 2 (dashed line), and the *ab initio* model (dot-dash line), respectively.

photodissociation,[41] where the $Cl(^2P_{3/2})$ produced from HCl is strongly aligned [c.f., $\mathbf{a}_0^{(2)}(\perp)$], while that produced from DCl exhibits essentially no alignment, i.e., $\mathbf{a}_0^{(2)}(\perp)\approx 0$.

Figure 6 illustrates the $\mathbf{a}_2^{(K)}(\perp)$ parameters as a function of photolysis energy for the ground-state $I(^2P_{3/2})$ fragment resulting from the dissociation of DI. Unlike what is seen for the $\mathbf{a}_0^{(K)}(\perp)$ parameters, there are fairly significant differences between the $\mathbf{a}_2^{(K)}(\perp)$ parameters for HI and DI for a given model, compare Figs. 3 and 6. The difference between the $\mathbf{a}_2^{(K)}(\perp)$ parameters predicted from model 1 and the *ab initio* model is also quite large for all photolysis energies and, thus, the more appropriate model could be verified experimentally.

The angular distribution of the excited-state iodine fragment $I(^2P_{1/2})$ resulting from dissociation of DI is described by the $\mathbf{a}_0^{(1)}(\perp)$ and $\mathbf{a}_1^{(1)}(\parallel,\perp)$ parameters. As with HI, the $\mathbf{a}_0^{(1)}(\perp)$ parameter is equal to the maximal value of 0.577 for all photolysis energies. Figure 7 plots the $\mathrm{Re}[\mathbf{a}_1^{(1)}(\parallel,\perp)]$ and $\mathrm{Im}[\mathbf{a}_1^{(1)}(\parallel,\perp)]$ parameters for all three empirical models. For model 0, the $\mathrm{Re}[\mathbf{a}_1^{(1)}(\parallel,\perp)]$ parameters for $I(^2P_{1/2})$ produced from HI and DI are similar across the entire energy range

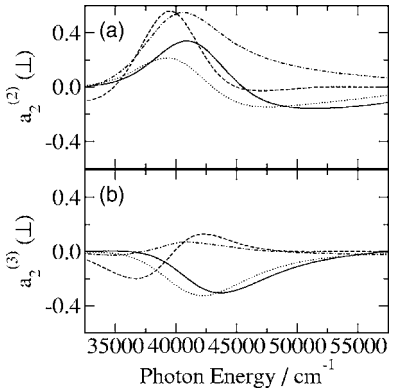

FIG. 6. Coherent anisotropy parameters (a) $\mathbf{a}_2^{(2)}(\perp)$ and (b) $\mathbf{a}_2^{(3)}(\perp)$ for the production of ground state $I(^2P_{3/2})$ as a function of photon energy for the photodissociation of DI initially in the rotationless ground $(v=0)$ vibrational state. The results were determined from model 0 (solid line), model 1 (dotted line), model 2 (dashed line), and the *ab initio* model (dot-dash line), respectively.

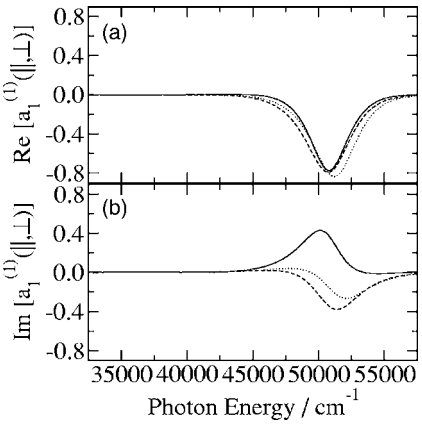

FIG. 7. Coherent anisotropy parameters (a) $\mathrm{Re}[\mathbf{a}_1^{(1)}(\|,\perp)]$ and (b) $\mathrm{Im}[\mathbf{a}_1^{(1)}(\|,\perp)]$ for the production of excited state $\mathrm{I}(^2P_{1/2})$ as a function of photon energy for the photodissociation of DI initially in the rotationless ground ($v=0$) vibrational state. The results were determined from model 0 (solid line), model 1 (dotted line), and model 2 (dashed line), respectively.

illustrated while there are fairly significant differences for models 1 and 2 for photolysis energies between 47 500 and 52 500 cm^{-1}. For models 1 and 2, the maximal value of $\mathrm{Re}[\mathbf{a}_1^{(1)}(\|,\perp)]$, occurring at approximately 50 000 cm^{-1}, is larger for DI than for HI. The calculated $\mathrm{Im}[\mathbf{a}_1^{(1)}(\|,\perp)]$ parameters from HI and DI exhibit opposite signs for model 0 while they are of the same sign for models 1 and 2. The difference between $\mathrm{Im}[\mathbf{a}_1^{(1)}(\|,\perp)]$ parameters for HI and DI could be measured experimentally. The $\mathrm{Im}[\mathbf{a}_1^{(1)}(\|,\perp)]$ parameter is dependent on the sine of the phase difference of the radial wave functions created on the $a\ ^3\Pi_{0^+}$ and $t\ ^3\Sigma_1$ states, i.e., $\sin\Delta\phi$, modulated by the transition amplitudes for these transitions.[43,44] On the other hand, the $\mathrm{Re}[\mathbf{a}_1^{(1)}(\|,\perp)]$ parameter has a $\cos\Delta\phi$ dependence. Therefore, the differences between HI and DI reflect these differences and measurement of the $\mathbf{a}_1^{(1)}(\|,\perp)$ parameters will provide a detailed information regarding the $a\ ^3\Pi_{0^+}$ and $t\ ^3\Sigma_1$ states.

The calculated differences between HI and DI await experimental verification. If verified, they could provide additional confirmation of one of the current models of adiabatic photodissociation for HI or would allow refinement of the models.

IV. CONCLUSIONS

We have reexamined the photodissociation of HI and DI using time-dependent wave-packet dynamics based on the recent empirical models (models 1 and 2, see Tables II and III) for the potential-energy curves and transition dipole moment functions of Camden *et al.*[21] and based on the best available *ab initio* data.[24] In particular, the focus has been on determining the (near) complete set of anisotropy parameters $\mathbf{a}_Q^{(K)}(p)$ describing the $\mathrm{I}(^2P_{3/2})$ and $\mathrm{I}(^2P_{1/2})$ angular momentum distributions arising from the photodissociation of HI and DI as a function of photon energy.[71] These results have been compared to each other and contrasted to ones[42] determined using the original model[22] of LeRoy *et al.* (model 0, see Table I). We demonstrate that measurement of the anisotropy parameters for the excitation from $v=0$ will be able to distinguish between the two empirical models that were recently developed to account for the measurements from $v=2$ and the *ab initio* data; their measurement could also distinguish model 0, which did not properly reproduce the data for vibrationally mediated photodissociation. While there are experimental difficulties associated with the measurement of $\mathbf{a}_Q^{(K)}(p)$, including the depolarization of the iodine fragments, they will provide an alternative to the vibrationally mediated photodissociation experiments proposed.[21] In our recent study of HI and DI photodissociation,[42] predictions were made regarding the production of both highly spin-polarized H and D atoms from the dissociation of HI and DI. Within the current adiabatic treatment of the dissociation dynamics, *all* models predict that spin-polarized hydrogen and deuterium can be produced for energies below approximately 37 500 cm^{-1} and between 47 500 and 52 500 cm^{-1}, see discussion in Ref. 42 for further details.

Calculations of the anisotropy parameters have also been performed for photodissociation of vibrationally excited HI and DI in the $v=1$, 2, 3, and 4 states, although the results that have been presented are only for the excitation from $v=0$. Sharp changes in the vector properties discussed in this work are observed over narrow energy ranges due to the nodes in the initial vibrational state as have been theoretically determined for other properties, e.g., branching fractions and total cross sections, for the vibrationally mediated photodissociation of the hydrogen halides.[4,12,15,19,21,24,72] As with the scalar properties,[21] there are clear differences between the predictions of the $\mathbf{a}_Q^{(K)}(p)$ parameters based on various models for the electronic structure. To date, no experimental measurements of the $\mathbf{a}_Q^{(K)}(p)$ parameters from vibrationally mediated photodissociation have been obtained for the hydrogen halides.

The recent experimental work of Camden *et al.* on HI has shown that vibrationally mediated photodissociation provides a sensitive probe of repulsive excited states. However, the present study clearly demonstrates the sensitivity of vector properties to the details of the electronic structure. The four models of the excited states and transition dipole moments, each of which gives similar results for the scalar properties for the excitation from $v=0$, exhibit significant, and, more importantly, experimentally measurable differences in their vector properties.

ACKNOWLEDGMENTS

The authors thank the Natural Sciences and Engineering Research Council of Canada and the University of Alberta for financial support. One of the authors (A.B.) thanks Dr. A. Alekseyev (Bergische Universität Wuppertal) for providing the *ab initio* potential-energy data.

[1] J. Zhang, C. W. Riehn, M. Dulligan, and C. Wittig, J. Chem. Phys. **104**, 7027 (1996).
[2] A. Brown and G. G. Balint-Kurti, J. Chem. Phys. **113**, 1870 (2001).
[3] B. M. Cheng, C. Y. Chung, M. Bahou, Y. P. Lee, and L. C. Lee, J. Chem. Phys. **117**, 4293 (2002).
[4] P. M. Regan, D. Ascenzi, A. Brown, G. G. Balint-Kurti, and A. J. Orr-Ewing, J. Chem. Phys. **112**, 10259 (2000).
[5] S. Lee and K. H. Jung, J. Chem. Phys. **112**, 2810 (2000).

[6] Y. Li, O. Bludsky, G. Hirsch, and R. J. Buenker, J. Chem. Phys. **112**, 260 (2000).
[7] P. M. Regan, S. R. Langford, D. Ascenzi, P. A. Cook, A. J. Orr-Ewing, and M. N. R. Ashfold, Phys. Chem. Chem. Phys. **1**, 3247 (1999).
[8] D. Ascenzi, P. M. Regan, and A. J. Orr-Ewing, Chem. Phys. Lett. **310**, 477 (1999).
[9] H. M. Lambert, P. J. Dagdigian, and M. H. Alexander, J. Chem. Phys. **108**, 4460 (1998).
[10] J. Zhang, M. Dulligan, and C. Wittig, J. Chem. Phys. **107**, 1403 (1997).
[11] T. Duhoo and B. Pouilly, J. Chem. Phys. **103**, 182 (1995).
[12] I. H. Gersonde, S. Henning, and H. Gabriel, J. Chem. Phys. **101**, 9558 (1994).
[13] M. H. Alexander, B. Pouilly, and T. Duhoo, J. Chem. Phys. **99**, 1752 (1993).
[14] K. Tonokura, Y. Matsumi, M. Kawasaki, S. Tasaki, and R. Bersohn, J. Chem. Phys. **97**, 8210 (1992).
[15] S. C. Givertz and G. G. Balint-Kurti, J. Chem. Soc., Faraday Trans. 2 **82**, 1231 (1986).
[16] E. van Dishoeck, M. van Hemert, and A. Dalgarno, J. Chem. Phys. **77**, 3693 (1982).
[17] R. Baumfalk, U. Buck, C. Frischkorn, N. H. Nahler, and L. Hüwel, J. Chem. Phys. **111**, 2595 (1999).
[18] P. M. Regan, S. R. Langford, A. J. Orr-Ewing, and M. N. R. Ashfold, J. Chem. Phys. **110**, 281 (1999).
[19] B. Pouilly and M. Monnerville, Chem. Phys. **238**, 437 (1998).
[20] G. Peoux, M. Monnerville, T. Duhoo, and B. Pouilly, J. Chem. Phys. **107**, 70 (1997).
[21] J. P. Camden, H. A. Bechtel, D. J. A. Brown, A. E. Pomerantz, R. N. Zare, and R. J. LeRoy, J. Phys. Chem. A **108**, 7806 (2004).
[22] R. J. LeRoy, G. T. Kraemer, and S. Manzhos, J. Chem. Phys. **117**, 9353 (2002).
[23] S. Manzhos, H. P. Loock, B. L. G. Bakker, and D. H. Parker, J. Chem. Phys. **117**, 9347 (2002).
[24] A. B. Alekseyev, H. P. Liebermann, D. B. Kokh, and R. J. Buenker, J. Chem. Phys. **113**, 6174 (2000).
[25] P. M. Regan, D. Ascenzi, C. Clementi, M. N. R. Ashfold, and A. J. Orr-Ewing, Chem. Phys. Lett. **315**, 187 (1999).
[26] S. R. Langford, P. M. Regan, A. J. Orr-Ewing, and M. N. R. Ashfold, Chem. Phys. **231**, 245 (1998).
[27] D. J. Gendron and J. W. Hepburn, J. Chem. Phys. **109**, 7205 (1998).
[28] A. J. R. Heck and D. W. Chandler, Annu. Rev. Phys. Chem. **46**, 335 (1995).
[29] T. N. Kitsopoulos, M. A. Buntine, D. P. Baldwin, R. N. Zare, and D. W. Chandler, Proc. SPIE **1858**, 2 (1993).
[30] I. Levy and M. Shapiro, J. Chem. Phys. **89**, 2900 (1988).
[31] Z. Xu, B. Koplitz, and C. Wittig, J. Phys. Chem. **92**, 5518 (1988).
[32] C. A. Wight and S. R. Leone, J. Chem. Phys. **79**, 4823 (1983).
[33] G. N. A. van Veen, K. A. Mohamed, T. Baller, and A. E. deVries, Chem. Phys. **80**, 113 (1983).
[34] R. Schmiedl, H. Dugan, W. Meier, and K. H. Welge, Z. Phys. A **304**, 137 (1982).
[35] R. D. Clear, S. J. Riley, and K. R. Wilson, J. Chem. Phys. **63**, 1340 (1975).
[36] C. E. Moore, *Atomic Energy Levels* (U.S. Government Printing Office, Washington, DC, 1971).
[37] T. P. Rakitzis, P. C. Samartzis, R. L. Toomes *et al.*, Chem. Phys. Lett. **364**, 115 (2002).
[38] T. P. Rakitzis, P. C. Samartzis, R. L. Toomes, T. N. Kitsopoulos, A. Brown, G. G. Balint-Kurti, O. S. Vasyutinskii, and J. A. Beswick, Science **300**, 1936 (2003).
[39] T. P. Rakitzis, P. C. Samartzis, R. L. Toomes, and T. N. Kitsopoulos, J. Chem. Phys. **121**, 7222 (2004).
[40] G. G. Balint-Kurti, A. J. Orr-Ewing, J. A. Beswick, A. Brown, and O. S. Vasyutinskii, J. Chem. Phys. **116**, 10760 (2002).
[41] A. Brown, G. G. Balint-Kurti, and O. S. Vasyutiniskii, J. Phys. Chem. A **108**, 7790 (2004).
[42] A. Brown, J. Chem. Phys. **122**, 084301 (2005).
[43] L. D. A. Siebbeles, M. Glass-Maujean, O. S. Vasyutinskii, J. A. Beswick, and O. Roncero, J. Chem. Phys. **100**, 3610 (1994).
[44] T. P. Rakitzis and R. N. Zare, J. Chem. Phys. **110**, 3341 (1999).
[45] B. V. Picheyev, A. G. Smolin, and O. S. Vasyutinskii, J. Phys. Chem. A **101**, 7614 (1997).
[46] E. R. Wouters, M. Ahmed, D. S. Peterska, A. S. Bracker, A. G. Suits, and O. S. Vasyutinskii, in *Imaging in Chemical Dynamics*, edited by A. G. Suits and R. E. Continetti (American Chemical Society, Washington, DC, 2000), p. 238.
[47] A. B. Alekseyev, D. B. Kokh, and R. J. Buenker, J. Phys. Chem. A **109**, 3094 (2005).
[48] N. Balakrishnan, A. B. Alekseyev, and R. J. Buenker, Chem. Phys. Lett. **341**, 594 (2001).
[49] A. S. Bracker, E. R. Wouters, A. G. Suits, and O. S. Vasyutinskii, J. Chem. Phys. **110**, 6749 (1999).
[50] C. F. Goodeve and A. W. C. Taylor, Proc. R. Soc. London **A154**, 181 (1936).
[51] J. Romand, Ann. Phys. (Paris) **4**, 527 (1948).
[52] J. F. Ogilvie, Trans. Faraday Soc. **67**, 2205 (1971).
[53] D. A. Chapman, K. Balasubramanian, and S. H. Lin, Chem. Phys. Lett. **118**, 192 (1985).
[54] D. A. Chapman, K. Balasubramanian, and S. H. Lin, J. Chem. Phys. **87**, 5325 (1987).
[55] D. A. Chapman, K. Balasubramanian, and S. H. Lin, Phys. Rev. A **38**, 6098 (1988).
[56] J. A. Coxon and P. G. Hajigeorgiou, J. Mol. Spectrosc. **150**, 1 (1991).
[57] R. N. Zare, *Angular Momentum* (World Scientific, New York, 1988).
[58] A. R. Edmonds, *Angular Momentum in Quantum Mechanics* (Princeton University Press, Princeton, 1960).
[59] G. G. Balint-Kurti, R. N. Dixon, and C. C. Marston, Int. Rev. Phys. Chem. **11**, 317 (1992).
[60] G. G. Balint-Kurti, R. N. Dixon, and C. C. Marston, J. Chem. Soc., Faraday Trans. **86**, 1741 (1990).
[61] E. J. Heller, J. Chem. Phys. **68**, 2066 (1978).
[62] E. J. Heller, J. Chem. Phys. **68**, 3891 (1978).
[63] E. J. Heller, Acc. Chem. Res. **14**, 368 (1981).
[64] G. G. Balint-Kurti, Adv. Chem. Phys. **128**, 249 (2003).
[65] A. Brown and G. G. Balint-Kurti, J. Chem. Phys. **113**, 1879 (2001).
[66] In recent work [V. V. Kuznetsov and O. S. Vasyutinskii, J. Chem. Phys. **123**, 034307 (2005)], the role of molecular axis rotation on the photofragment angular momentum distributions has been considered. For low to moderate rotational states, the Coriolis nonadiabatic interaction should be negligible for the hydrogen halides, see, for example, Refs. 13 and 19. Neglecting the Coriolis nonadiabatic interaction, the molecular frame anisotropy parameters do not depend on the rotation of the molecular axis.
[67] C. C. Marston and G. G. Balint-Kurti, J. Chem. Phys. **91**, 3571 (1989).
[68] G. G. Balint-Kurti, C. L. Ward, and C. C. Marston, Comput. Phys. Commun. **67**, 285 (1991).
[69] H. Tal-Ezer and R. Kosloff, J. Chem. Phys. **81**, 3967 (1984).
[70] R. Kosloff, J. Phys. Chem. **92**, 2087 (1988).
[71] See EPAPS Document No. E-JCPSA6-123-024527 for the numerical data contained in Figs. 2–7, i.e., the anisotropy parameters for $I(^2P_{3/2})$, $I(^2P_{1/2})$, and H/D produced from the photodissociation of HI and DI as a function of photolysis energy. This document can be reached via a direct link in the online article's HTML reference section or via the EPAPS homepage (http://www.aip.org/pubservs/epaps.html).
[72] C. Kalyanaraman and N. Sathyamurthy, Chem. Phys. Lett. **209**, 52 (1993).